PCCP

Accepted Manuscript




ROYAL SOCIETY OF CHEMISTRY

www.rsc.org/pccp

Journal Name

RSCPublishing

ARTICLE

# Enhanced Field Emission from In-situ Synthesized 2D Copper Sulfide Nanoflakes at Low Temperature by Using a Novel Controllable Solvothermal Preferred Edge Growth Route

Cite this: DOI: 10.1039/xoxxoooooox

Received ooth January 2012,
Accepted ooth January 2012

DOI: 10.1039/xoxxoooooox

www.rsc.org/

Zengcai Song [a,b], Hongwei Lei[a], Borui Li[a], Haoning Wang[a], Jian Wen[a], Songzhan Li[a], Guojia Fang [a,b] *

ABSTRACT: A facile one-pot solvothermal route using the reaction of sputtered copper film and sulfur powder in ethanol solution at a low temperature of 90°C for 12 hours has been implemented to in-situ synthesize 2D hexagonal copper sulfide (CuS) nanoflakes. Their field electron emission (FE) characteristics were investigated and were found having close relationship with the copper film's thickness. The lowest turn on electric field ($E_{on}$) was 2.05 V/μm and the largest field enhancement factor (β) was 7261 when the copper film' thickness was 160 nm. Furthermore, through a preferred edge growth route, patterned CuS nanoflakes were synthesized with the combined effect from a copper film seed layer and a passivation layer to further improve FE properties with $E_{on}$ of 1.65 V/μm and β of 8351. The mechanism of the patterned CuS nanoflakes preferred edge growth is firstly reported and discussed.

## Introduction

In the past few years, low dimensional nanostructures (nanowalls, nanotubes, nanowires, nanoparticles etc.) and low dimensional heterojunction structures based on all kinds of nanomaterials have attracted a great deal of interest for both scientific fundamentals in nanoscience[1] and potential applications in nanoscale systems, including various new electronic and photonic nanodevices[2-4]. Among various low dimensional nanostructural materials, 2D transition metal sulfides are the most studied materials[5-8] because of their large carrier mobility, good electrical conductivity and so on. Among them, copper sulfides are a class of functional semiconductors with many different structures and components, including covellite CuS, anilite $Cu_{1.75}S$, digenite $Cu_{1.8}S$, djurleite $Cu_{1.95}S$, chalcocite $Cu_2S$ and so on.

Their complex structures and valence states, together with their low cost and low toxicity, result in their great potential applications in super-capacitors[9], solar cells[10], lithium ion batteries[11], photocatalysis[12], biomedical and environmental fields[13-14]. Besides, field electron emission is also an important phenomenon for its application in flat-panel displays, high energy accelerators, X-ray sources, microwave amplifiers and vacuum microelectronic devices.[15-18] Field emission properties of $MoS_2$ as representation of transition metal sulfides have been investigated widely.[19-22] However, as a great member of transition metal sulfides there are still rare reports about the field emission performance of 2D CuS nanoflakes.[23-25] Much more works on CuS referring other excellent field emission (FE) materials such as CNT[26] could be done to improve their field electron emission properties in three aspects: i) reduce turn on and threshold electric field: ii) increase emission current; iii) improve the stability of emission current. Generally speaking, high temperature process is needed for the synthesis of those FE materials such as CVD CNTs.

In this article, we report a facile one-pot solvothermal route for in-situ growth of 2D CuS nanoflakes at a low temperature of 90°C. This method has various advantages including simplicity, environmentally friendly, energy saving and so on which is similar to the method used to synthesize copper oxide nanostructures[27]. More importantly, a conventional photolithography followed by lift-off techniques is used to produce patterned and fence-like CuS nanoflakes realizing their preferred edge growth which is never reported before to the best of our knowledge and the growth mechanism of the patterned CuS nanoflakes is discussed. Their field emission performance is investigated with some interesting results of pretty low turn-on electric field (1.65 V/μm) and high field enhancement factor (8351) which is much more improved than before. In one word, our work investigates the structures of 2D CuS nanoflakes, along with their field emission properties, with the purpose of determining a structure-property relationship.

## Experimental

**Materials and Synthesis**

All primitive materials were purchased from commercial sources and used without further purification. The substrates used in our experiment were n-type silicon (Si) wafers whose electrical resistivity was $9.0\times10^{-3}$ Ω•cm. They had been cleaned using Radio Corporation of America (RCA) method in order to remove original oxide layer and further ultrasonic cleaned sequentially with acetone, alcohol, deionized water and blew dried with dry $N_2$ before deposition. Copper film was then deposited on Si wafer by a radio frequency (RF) reactive magnetron sputtering system using a copper (99.9% purity) target. The deposition time was controlled to 15s, 30s, 60s, 90s, 120s and 150s. The approximate thicknesses of copper films calculated from Cu deposition rate are 20, 40, 80, 120, 160 and 210nm.

After that, a novel solvothermal route was implemented to grow 2D CuS nanoflakes as follows. Substrates coated by copper film and 60 mg sulfur powder were put into a teflon lined autoclave. After 40 mL ethanol was poured into, the autoclave was sealed and maintained at 90°C for 12 hours and then allowed to cool to room temperature. The resulting residues were washed sequentially with de-ionized water and ethanol to remove unreacted impurities. The nanoflakes were dried at 60°C for 2 hours in air at last.

On the other hand, patterned CuS nanoflakes arrays were also fabricated through a preferred edge growth method. 160 nm-thick copper films coated without or with passivation layer (sputtered ITO, 40nm) were treated with a conventional photolithography followed by lift-off techniques causing the whole film to be divided into patterned cylindrical arrays (diameter: 20 μm) before growing CuS nanoflakes. Then CuS nanoflakes grew under the same condition mentioned above.

**Sample Characterization**

The morphology of CuS nanoflakes was characterized by field emission scanning electron microscope (FESEM, FEI XL-30) together with an energy-dispersive X-ray spectroscopy (EDS) and transmission electron microscope (TEM). TEM techniques, including the bright field (BF) imaging and the selected area electron diffraction (SAED), were performed using a JEOL JEM-2010 electron microscope. The X-ray diffraction (XRD) pattern was acquired using a Burker Axs, D8 Advance with Cu Kα radiation at 40 kV and 40 mA. The compositions and chemical states of the CuS nanoflakes were examined by X-ray photoelectron spectroscopy (XPS) and ultraviolet photoelectron spectroscopy (UPS) by a Thermo Scientific ESCLAB 250 Xi with Al Kα X-ray source (hλ=1486.68 eV).

The field emission characteristics were investigated in a home-made vacuum chamber with a base pressure of $2.0\times10^{-5}$ Pa under a two-parallel-plate configuration as shown in Fig. S1. The samples were fixed onto the cathode, while another parallel ITO glass plate served as the anode. The cathode area was 0.2 cm × 0.2 cm. The anode and cathode were separated by a 220 μm teflon spacer. A voltage supplied by a Keithley 248 high-voltage source was applied between the anode and cathode to supply an electric field. The emission current was monitored by a Keithley 6485 picoammeter. In order to obtain reliable emission current, we have performed electrical annealing on all our samples.

## Results and discussion

The field emission scanning electron micrographs of 2D CuS nanoflakes are shown in Fig. 1. Fig. 1a – 1f exhibit CuS nanoflakes named as Cu_15s, Cu_30s, Cu_60s, Cu_90s, Cu_120s and Cu_150s based on sputtering time of 15, 30, 60, 90, 120 and 150 seconds for different thick copper film deposition, respectively. As can be seen from these pictures, with the copper films becoming thicker, CuS nanoflakes are formed and grow up slowly but definitely. When the thickness of the sputtered copper film is less than 60 nm shown in Fig. 1a and 1b, copper film reacts with sulfur powder forming a small amount of CuS nanoflakes which can be known from the bare part of substrate. If the thicknesses are more than 60 nm, CuS nanoflakes can carpet the whole substrate and the samples' surface becomes smoother as Cu films become thicker which can be seen from Fig. 1c – 1e. Furthermore, as the thickness becomes to more than 160 nm, CuS nanoflakes further grow up and the size of CuS nanoflakes almost reach to 500 nm as shown in Fig. 1f. Additionally, higher magnification SEM images of these samples with 100 nm scale bars are shown in the inset of Fig. 1. The thickness of CuS nanoflakes is around 10 nm. The density and size of CuS nanoflakes are becoming larger as the increase of copper films' thicknesses. The yield of product CuS nanoflakes increases with the increase of the copper films' thickness. When copper film' thickness is 160nm, copper film reacts with sulfur powder completely which can be confirmed by energy-dispersive X-ray spectroscopies (Fig. S2). If copper film is becoming thicker than 160 nm, copper film will be residual after reaction which leads to the similarity of morphological variation as shown in Fig. 1e and 1f.

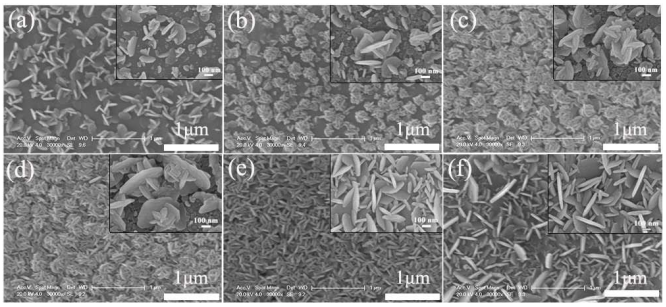


Fig. 1 SEM micrographs of CuS nanoflakes based on sputtered copper film with the thickness of (a) 20 nm, (b) 40 nm, (c) 80 nm, (d) 120 nm, (e) 160 nm and (f) 210 nm. Inset: higher magnification SEM images with 100 nm scale bars.

The energy-dispersive X-ray spectroscopies (EDS) of four samples (Cu_30s, Cu_60s, Cu_90s, Cu_120s and Cu_150s) are depicted in Fig. S2. It's difficult to obtain EDS spectrum in sample Cu_15s because of its small amount of CuS nanoflakes. As can be seen from Fig. S2, the atomic ratios of Cu and S elements of all the samples are nearly to 1.0. In sample Cu_120s, the atomic ratio of Cu and S elements is the most



 

close to 1.0. The Raman spectra of all the samples are observed and some of the results for samples Cu_60s, Cu_90s, Cu_120s and Cu_150s are presented in Fig. S2. All the spectra only have one peak at the same position (~475 $cm^{-1}$) besides the effect of Si substrate. The band at 475 $cm^{-1}$ in CuS nanoflakes revealing that the lattice atoms of CuS are aligned in the periodic array, agrees well with the observation for the covellite structure of CuS with a hexagonal crystal structure. The observed Raman-active modes of CuS nanoflakes are consistent with previously reported data.[28] As can be seen from these results, the component of our products is covellite CuS.

The microstructure and chemical composition of CuS nanoflakes of sample Cu_120s are investigated with transmission electron microscope (TEM) accompanied by selected area electron diffraction (SAED). CuS nanoflakes were scraped from the samples' surface and ultrasonic dispersed in alcohol for TEM analysis and the corresponding SAED analysis, as shown in Fig. 2a and 2b. The CuS nanoflakes have a hexagonal crystal phase from the TEM observation and are single-crystalline for the appearance of diffraction dots in the SAED pattern. What's more, a typical XRD pattern of the product is shown in Fig. 2c, which can be indexed to be hexagonal phase CuS in accordance with the results of the TEM analysis. The refined lattice constants are a = b = 3.792 Å and c = 16.344 Å, in accordance with the reported value for CuS crystal (JCPDS card, No. 06-0464).

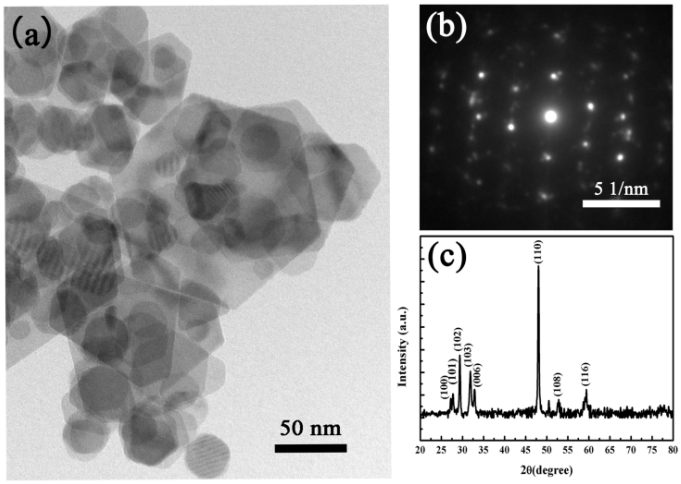


Fig. 2 (a) TEM image, (b) SAED pattern and (c) XRD pattern of CuS nanoflakes of sample Cu_120s.

Important information on the surface electronic state and the composition of the products can be further provided by X-ray photoelectron spectroscopy (XPS) and ultraviolet photoelectron spectroscope (UPS) as shown in Fig. 3. Fig. 3b and 3c are high resolution XPS spectra of Cu 2p and S 2p peaks. The binding energies of Cu $2p_{3/2}$ and Cu $2p_{1/2}$ peaks at 932.1 eV and 952.0 eV are shown in Fig. 3b respectively, which are typical values of $Cu^{2+}$ in CuS. In the S 2p region, a double peak located at 162.5 eV in another high resolution spectrum (Fig. 3c) corresponds to S 2p orbital which is a typical value for metal sulfides. The spectral deconvolution of the S 2p bands with a Gaussian profile reveals two sets of S 2p doublets and the presence of sulfur. Through an analysis of the relative intensity of Cu and S peaks, it can be calculated that the Cu/S ratio is 2:3 which is less than the stoichiometry 1.0 of CuS. This might due to the residual of sulfur powder on the sample surfaces. UPS analysis is employed to further determine work function of the prepared CuS nanoflakes, as shown in Fig. 3d. From the UPS results, the work function of CuS is obtained from the intersection point of the tangent line (black line in Fig. 3d) and x-axis with its value of 4.95 eV.

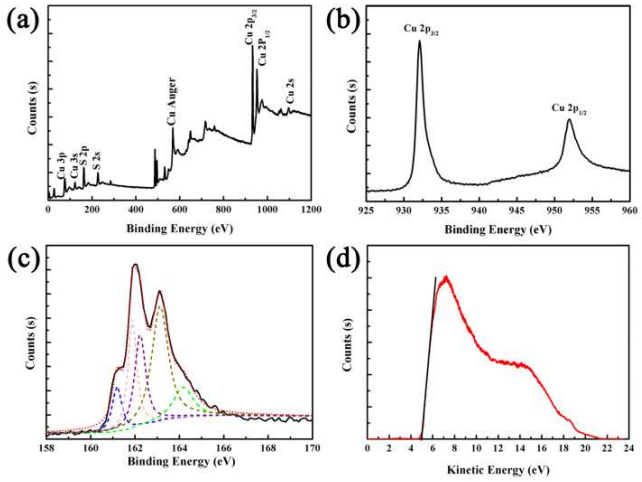


Fig. 3 Typical XPS spectra of the CuS nanoflakes: (a) survey spectrum, (b) Cu 2p region XPS spectrum, and (c) S 2p region XPS spectrum. The solid line represents the experimental data, and the dashen and dotted lines represent spectral deconvolution results. (d) UPS analysis of CuS nanoflakes.

The field emission characteristics of our CuS nanoflakes are shown in Fig. 4. Field emission from in-situ synthesized CuS nanoflakes is observed noticeably up to the maximum applied electric field of 11.2 V/μm. FE current density versus electric field (J-E) characteristics of samples are illustrated in Fig. 4a. The typical electric fields for obtaining current density of 10 μA/$cm^2$ and 100 μA/$cm^2$ are defined as turn-on electric field ($E_{on}$) and threshold electric field ($E_{th}$). As the Cu film's thickness increased from 20 to 210 nm, the turn-on electric fields of CuS nanoflakes decreased first and then increased, from 9.54 V/μm (20 nm) to 2.05 V/μm (160 nm) then to 2.70 V/μm (210 nm). The same law is found to threshold electric fields which decreased from 7.20 V/μm (40 nm) to 3.07 V/μm (160 nm) then increased to 3.52 V/μm (210nm).

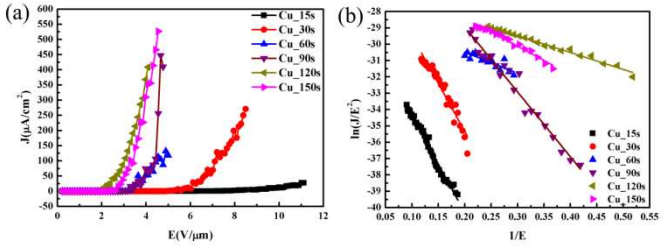


Fig. 4 (a) FE current density vs. electric field plots for CuS nanoflakes of all the samples Cu_15s, Cu_30s, Cu_60s, Cu_90s, Cu_120s and Cu_150s. (b) The FN plots of the field emission J-E characteristic curves.

According to the F-N equation

$$J = A\frac{\beta^2 E^2}{\varphi}\exp(-\frac{B\varphi^{3/2}}{\beta E}),$$

where J is the field emission current density, E is the applied electrical field, A, B are constants, A = $1.56\times10^{-10}$ $AV^{-2}eV$, B = $6.83\times10^{3}$ $VeV^{-3/2}$ $\mu m^{-1}$, β is the field enhancement factor and φ is the work function (4.95 eV for CuS known from UPS result) of the material, the FN plot, $\ln(I/E^2)$ vs 1/E, is expected to be a straight line. The slop of FN plot has an inverse ratio to the field enhancement factor β, which is given by

$$k = -\frac{B\varphi^{3/2}}{\beta},$$

where k stands for slop. The corresponding FN plot of the data in Fig. 5a is shown in Fig. 5b. The field enhancement factors of CuS nanoflakes increased from 1258 to 7261 then decreased to 4322 having a similar rule with $E_{on}$ and $E_{th}$. The detailed parameters of the field emission properties are shown in Table 1.

Table 1 Detailed Parameters of the Field Emission Properties for Samples Based on Different Thick Copper Films

| Samples | Copper film's thickness/nm | $E_{on}$/V·μm$^{-1}$ | $E_{th}$/V·μm$^{-1}$ | F-N slop | β |
|---|---|---|---|---|---|
| Cu_15s | 20 | 9.54 | | -59.7710 | 1258 |
| Cu_30s | 40 | 5.85 | 7.20 | -58.6365 | 1283 |
| Cu_60s | 80 | 3.35 | 4.89 | -12.9193 | 5822 |
| Cu_90s | 120 | 3.26 | 4.43 | -39.7342 | 1893 |
| Cu_120s | 160 | 2.05 | 3.07 | -10.3590 | 7261 |
| Cu_150s | 210 | 2.70 | 3.52 | -17.4031 | 4322 |

β stands for field enhancement factor.

According to the results above, the field emission properties of CuS nanoflakes based on 160 nm-thick sputtered copper film performed the best. To further overcome electric field screen effect and improve field emission properties, another experiment was performed realizing CuS nanoflakes preferred edge growth for the first time and decreasing the screen effect evidently. 160 nm-thick copper film with or without passivation layer (sputtered ITO) was treated with a conventional photolithography followed by lift-off techniques causing the whole film to be etched into cylindrical arrays before growing CuS nanoflakes. After growing CuS nanoflakes, SEM images of the special structures are shown in Fig. 5. Around the edge of cylinders CuS nanoflakes are obviously higher than those grown inside forming fence-like structures. From the high resolution SEM images, CuS nanoflakes only grew along the edge of those cylinders due to ITO passivation layer (Fig. 5e and 5f). While if there was no ITO passivation layer CuS nanoflakes would also grow inside those cylinders (Fig. 5b and 5c). CuS samples based copper films coated without or with passivation layer are named as Cu_120s_etched and Cu_120s_etched-ITO.

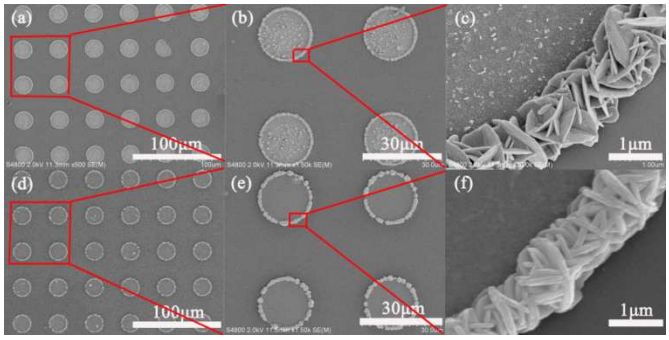


Fig. 5 Low and high resolution SEM images of the CuS nanoflakes based on the patterned copper film without (a, b and c) and with (d, e and f) ITO passivation layer.

Fig. 6 is a schematic drawing used to explain the formation of these fence-like structures properly. In the left picture, copper film without any treatment only reacts with sulfur powder dissolved in alcohol from its top position as the up arrow directed. While in the middle picture cylindrical copper film arrays without ITO passivation layer could react with sulfur from all directions except its bottom as the arrows directed. So for the CuS nanoflakes around the edge of cylindrical arrays their synthesis could be carried out from two directions including top and side leading to the fence-like structures (Fig. 5a – 5c)). Furthermore, if the patterned copper cylindrical arrays are covered with ITO passivation layer, copper would not react with sulfur from its top direction as the right picture shown in Fig. 6. In this case, CuS nanoflakes preferred edge growth are formed as shown in Fig. 5d – 5f.

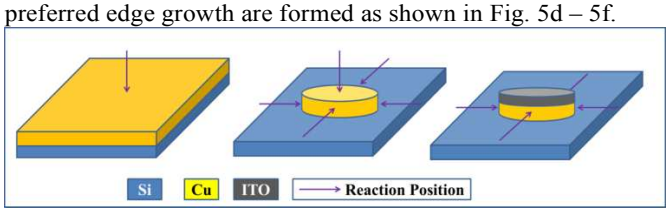


Fig. 6 Schematic diagram of the reaction between sulfur and copper film without (the left) and with (the middle: without ITO passivation layer, the right: with ITO passivation layer) being treated before.

Based on the results above, the CuS nanoflake structures of sample Cu_120s_etched shown in Fig. 5a - 5c are some kind of solid pattern arrays; while the structures of sample Cu_120s_etched-ITO shown in Fig. 5d – 5f are some kind of hollow pattern arrays. The field emission properties of CuS nanoflakes of the two different structures and no patterned structures are measured with the results shown in Fig. 7. The turn on and threshold electric field of solid patterned CuS nanoflakes from sample Cu_120s_etched derived from J-E characteristic are 1.82 V/μm and 2.39 V/μm, respectively, which are smaller than those of no patterned sample Cu_120s indicating the better performance shown in Table 2. In addition, hollow patterned CuS nanoflakes of sample Cu_120s_etched-ITO formed by preferred edge growth show better enhanced field emission properties with $E_{on}$ = 1.65 V/μm and $E_{th}$ = 2.21 V/μm, which are decreased by 0.40 V/μm and 0.86 V/μm than no patterned CuS nanoflakes, 0.17 V/μm and 0.18 V/μm than

solid patterned CuS nanoflakes respectively. It is noted that these values of the nanoflakes are comparable to many other inorganic semiconductor nanomaterials, such as CNT[29], SiC[30] and ZnO[31,32]. In addition, the value of $E_{on}$ (1.65 V/μm) for the in-situ synthesized hollow CuS nanoflakes arrays is much lower than that in Feng's work (8.5 V/μm)[23] and that for the copper sulphide ($Cu_2S$) nanowire arrays (11 V/μm)[25].

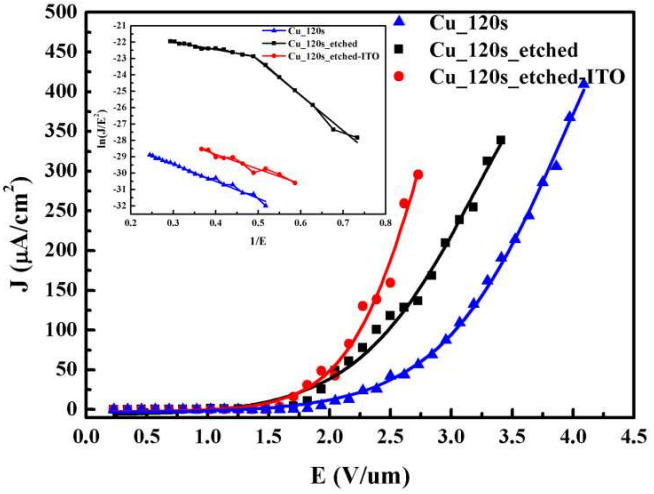


Fig. 7 FE current density vs. electric field plots for CuS nanoflakes of samples Cu_120s, Cu_120s_etched and Cu_120s_etched-ITO. Inset: The FN plots of the field emission J-E characteristic curves.

As shown in the inset of Fig. 7, the FN plots are straight lines and agree with FN theory perfectly indicating that the electron emission of the as-grown samples is a tunnelling and cold electron emission process. The slops of the straight lines are -10.3590 of Cu_120s and -9.0071 of Cu_120s_etched-ITO derived from the FN plots. Moreover, the field enhancement factor can be calculated from the slope of the ln(I/E2) -1/E plot as mentioned before, because of the work function of the emitter is known ($\varphi_{CuS}$ = 4.95 eV). It presents the estimated β value increases to 8351 for hollow patterned nanoflakes from 7261 for no patterned CuS nanoflakes in Table 2. At the same time, a two-stage slope behavior is observed in the FN plot for the solid patterned nanoflakes. Such two-stage slope characteristics are also reported in many other types of field emitters such as ZnO[33] and CNTs[34].

Table 2 Detailed Parameters of The Field Emission Properties for Different Patterned CuS Nanoflake Samples

| Samples | $E_{on}$/V·μm$^{-1}$ | $E_{th}$/V·μm$^{-1}$ | F-N slop | β |
|---|---|---|---|---|
| Cu_120s | 2.05 | 3.07 | -10.3590 | 7261 |
| Cu_120s_ etched | 1.82 | 2.39 | ----- | ----- |
| Cu_120s_ etched- ITO | 1.65 | 2.21 | -9.0071 | 8351 |

The enhanced field emission properties of CuS nanoflakes can be explained as below. The method using preferred edge growth route to diminish the screen effect of the ZnO nanorods synthesized by hydrothermal approach has been reported in our previous work[32]. It is also practical to enhance CuS nanoflakes' field emission properties using this method due to the results above. The structure of hollow patterned CuS nanoflakes diminishes the screen effect effectively which is in accordance with our simulation results.

The emission stability test of the typical sample Cu_120s_etched-ITO was performed at a preset current density value of ~250 μA/cm$^2$ with the result shown in Fig. 8 and the recording interval was 5 s. As shown in Fig. 8, the sample isn't observed obvious emission degradation for over 3600s. Additionally, the emission fluctuation is about ~ 8% for sample Cu_120s_etched-ITO which shows a good emission stability.

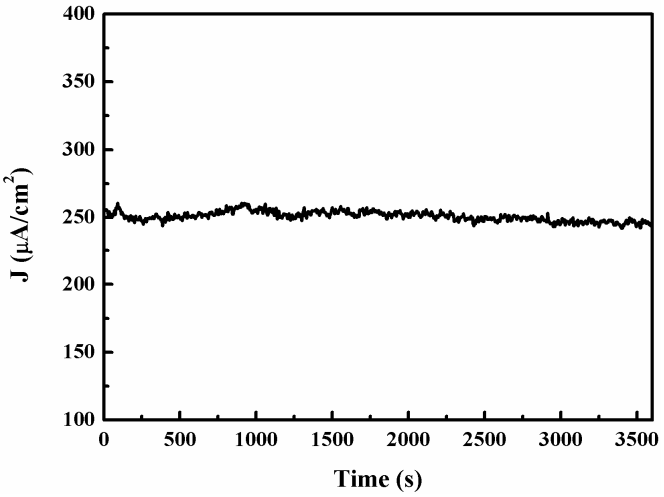


Fig. 8 The field emission current stability of CuS nanoflakes from sample Cu_120s_etch-ITO for over 3600 s.

## Conclusions

In conclusion, we have in-situ synthesized 2D copper sulfide (CuS) nanoflakes with a facile one-pot solvothermal route using the reaction of sputtered copper film and sulfur powder in ethanol solution at a low temperature of 90°C. The relationship between the morphology of CuS nanoflakes and the thickness of sputtered copper film was investigated. The field emission properties of our material were receiving major emphasis in this paper. The turn on electric field decreased to 2.05 V/μm and the field enhancement factor increased to 7261 through controlling the copper film's thickness of 160 nm. What's more, the CuS nanoflakes with preferred edge growth were synthesized with the combined effect from a copper film seed layer and an ITO passivation layer. The hollow patterned nanoflake structures diminished the screen effect in field emission effectively with a low turn on electric field of 1.65 V/μm and a high field enhancement factor of 8351. And CuS nanoflakes show good emission current stability over 3600 s. Our results imply that 2D CuS nanoflakes synthesized by solvothermal approach are promising candidates for vacuum electronic-device application.

## Acknowledgements

This work was financially supported by the National High Technology Research and Development Program (2015AA050601), the National Basic Research Program (No.2011CB933300) of China, the National Natural Science Foundation of China (61376013, 91433203, J1210061), the Natural Science Foundation of Jiangsu Province (BK20131186), the Suzhou Science & Technology Bureau

(SYG201449). We thank the nano center of Wuhan University for SEM and XRD measurements.

## Notes and references

[a] Department of Electronic Science and Technology and Key Laboratory of Artificial Micro- and Nano-structures of Ministry of Education, School of Physics and Technology, Wuhan University, Wuhan 430072, P. R. China. E-mail: gjfang@whu.edu.cn; Tel: +86-027-68752147
[b] Suzhou Institute of Wuhan University, Suzhou, 215123, P. R. China.
Electronic Supplementary Information (ESI) available: [details of any supplementary information available should be included here]. See DOI: 10.1039/b000000x/

1. D. Pan, M. Ombaba, Z.-Y. Zhou, Y. Liu and a. J. L. Shaowei Chen, *ACS Nano,* 2012, **6,** 10720-10726.
2. S. M. Hatch, J. Briscoe and S. Dunn, *Advanced Materials,* 2013, **25,** 867-871.
3. N. Liu, G. Fang, J. Wan, H. Zhou, H. Long and X. Zhao, *Journal of Materials Chemistry,* 2011, **21,** 18962.
4. S. K. Jha, C. Luan, C. H. To, O. Kutsay, J. Kováč, J. A. Zapien, I. Bello and S.-T. Lee, *Applied Physics Letters,* 2012, **101,** 211116.
5. M. Okada, T. Sawazaki, K. Watanabe, T. Taniguch, H. Hibino, H. Shinohara, R. Kitaura, *ACS Nano,* 2014, **8(8),** 8273-8277.
6. Y. H. Chang, W. Zhang, Y. Zhu, Y. Han, J. Pu, J. K. Chang, W. T. Hsu, J. K. Huang, C. L. Hsu, M. H. Chiu, T. Takenobu, H. Li, C. I. Wu, W. H. Chang, A. T. S. Wee, L. J. Li, *ACS Nano,* 2014, **8(8),** 8582-8590.
7. W. Liu, J. Kang, D. Sarkar, Y. Khatami, D. Jena, K. Banerjee, *Nano Letters,* 2013, **13,** 1983−1990.
8. X. Zou, J. Wang, C. H. Chiu, Y. Wu, X. Xiao, C. Jiang, W. W. Wu, L. Mai, T. Chen, J. Li, J. C. Ho, L. Liao, *Advanced Materials,* 2014, **26(36),** 6255-6261.
9. T. Zhu, B. Xia, L. Zhou and X. W. Lou, *Journal of Materials Chemistry,* 2012, **22,** 7851.
10. C. Wu, Z. Zhang, Y. Wu, P. Lv, B. Nie, L. Luo, L. Wang, J. Hu and J. Jie, *Nanotechnology,* 2013, **24,** 045402.
11. Y. Chen, C. Davoisne, J.-M. Tarascon and C. Guéry, *Journal of Materials Chemistry,* 2012, **22,** 5295.
12. M. Lee and K. Yong, *Nanotechnology,* 2012, **23,** 194014.
13. Q. Tian, M. Tang, Y. Sun, R. Zou, Z. Chen, M. Zhu, S. Yang, J. Wang, J. Wang and J. Hu, *Advanced Materials,* 2011, **23,** 3542-3547.
14. T. Fujimori and M. Takaoka, *Journal of Hazardous Materials,* 2011, **197,** 345-351.
15. W. Lei, C. Li, M. T. Cole, K. Qu, S. Ding, Y. Zhang, J. H. Warner, X. Zhang, B. Wang, W. I. Milne, *Carbon,* 2013, **56,** 255-263.
16. J. M. Kim, H. W. Lee, Y. S. Choi, J. E. Jung, N. S. Lee, Y. Y. Jin, N. S. Park, *Applied Surface Science,* 1999, **146,** 209-216.
17. H. H. Busta, J. M. Chen, Z. Shen, K. Jansen, S. Rizkowski, J. Matey, A. Lanzillotto, *Journal of Vacuum Science & Technology B,* 2003, **21(1),** 344-349.
18. S. Yamamoto, *Reports on Progress in Physics,* 2006, **69,** 181-232.
19. Y. B. Li, Y. Bando, D. Golberg, *Applied Physics Letters*, 2003, **82(12),** 1962-1964.
20. R. V. Kashid, D. J. Late, S. S. Chou, Y. K. Huang, M. De, D. S. Joag, M. A. More, V. P. Dravid, *Small,* 2013, **9(16),** 2730-2734.
21. D, J. Late, P. A. Shaikh, R. Khare, R. V. Kashid, M. Chaudhary, M. A. More, S. B. Ogale, *ACS Applied Materials & Interfaces,* 2014, **6,** 15881−15888.
22. Q, Zhang, K. Yu, B. Zhao, Y. Wang, C. Song, S. Li, H. Yin, Z. Zhang, Z. Zhu, *RSC Advances,* 2013, **3,** 10994–11000.
23. X. Feng, Y. Li, H. Liu, Y. Li, S. Cui, N. Wang, L. Jiang, X. Liu and M. Yuan, *Nanotechnology*, 2007, **18**, 145706.
24. B. Zhao, S. C. Li, Q. F. Zhang, Y. Wang, C. Q. Song, Z. L. Zhang, K. Yu, Chemical Engineering Journal, 2013, 230, 236-243.
25. J. Chen, S. Z. Deng, and N. S. Xu, *Applied Physics Letters,* 2002, **80,** 3620.
26. N. Perea-Lopez, B. Rebollo-Plata, J. A. Briones-Leon, A. Morelos-Gomez, D. Hernandez-Cruz, G. A. Hirata, V. Meunier, A. R. Botello-Mendez, J. C. Charlier, B. Maruyama, E. Munoz-Sandoval, F. Lopez-Urıas, M. Terrones, H. Terrones, *ACS Nano,* 2011, **5(6),** 5072-5077.
27. K. R. Khedir, Z. S. Saifaldeen, T. M. Demirkan, A. A. Al-Hilo, M. P. Brozak, T. Karabacak, *Advanced Engineering Materials,* doi: 10.1002/adem.201400397.
28. Z. Y. Zhan, C. Liu, L. X. Zheng, G. Z. Sun, B. S. Lia, Q. Zhang, *Physical Chemistry Chemical Physics*, 2011, 13, 20471−20475.
29. D. D. Nguyen, N. H. Tai, S. Y. Chen and Y. L. Chueh, *Nanoscale,* 2012, **4,** 632-638.
30. S. Chen, P. Ying, L. Wang, G. Wei, J. Zheng, F. Gao, S. Su and W. Yang, *Journal of Materials Chemistry C,* 2013, **1,** 4779.
31. Z. Song, H. Wei, Y. Liu, J. Wang, H. Long, H. Wang, P. Qin, W. Zeng, G. Fang, *IEEE Transactions on Nanotechnology,* 2014, **13,** 5.
32. N. Liu, G. Fang, W. Zeng, H. Long, L. Yuan and X. Zhao, *Applied Physics Letters,* 2009, **95,** 153505.
33. N. Liu, G. Fang, W. Zeng, H. Long, X. Zhao, *Journal of Physical Chemistry C,* 2011, **115,** 14377–14385.
34. Y. C. Choi, Y. M. Shin, D. J. Bae, S. C. Lim, Y. H. Lee, B. S. Lee, Diam. Relat. Mater. 2001, 10, 1457–1464.



 